JOURNAL OF Materials CHEMISTRY

Probing the chemical environment at the porous cage of ormosils through the fluorescence of oxazine 1

Francisco del Monte,[a] Maria L. Ferrer[a,b] and David Levy*[a,c]

[a]*Instituto de Ciencia de Materiales de Madrid-ICMM, Consejo Superior de Investigaciones Científicas-CSIC, Cantoblanco, 28049 Madrid, Spain. E-mail: D.Levy@icmm.csic.es*
[b]*Centro de Biología Molecular y Celular (División de Química-Física), Universidad Miguel Hernandez, Elche, 03202 Alicante, Spain*
[c]*Instituto Nacional de Tecnologia Aeroespacial-INTA, Laboratorio de Instrumentacion Espacial-LINES, Torrejon de Ardoz, 28850 Madrid, Spain*

Received 23rd November 2000, Accepted 20th March 2001
First published as an Advance Article on the web 25th April 2001

Ormosils (organically modified silicates) were prepared by the sol–gel process through the incorporation of non-ionic surfactants in the starting solution. Oxazine 1 was used as the fluorescent probe for the achievement of this study. Thus, recording of the absorption and emission fluorescence spectra, as well as measurement of the fluorescence lifetimes of oxazine 1, enabled us to determine the allocation of organic molecules within the porosity of silica gel-glasses. Furthermore, the reorientational correlation times of the fluorescent probe have been obtained through fluorescence anisotropy. According to the microviscosity data calculated from the fluorescent anisotropy measurements, movement of oxazine 1 is more restricted in the porous cage of ormosils than it is in silica gel-glasses.

Introduction

During the past 17 years, type 1 ormosils[1–6] have been widely prepared through the incorporation of organic additives along the sol–gel process.[7–11] It is well known that the incorporation of surfactants, oligomers or low molecular weight polymers modifies the final structure of the silica network (*e.g.* the incorporation of surfactants gives rise to the formation of mesoporous matrices, characterized by a network structure of ordered and uniform porosity[12,13]). On the other hand, optically active organic molecules (UV–VIS,[14] NIR[15] or photochromic[16] dyes, among others) can also be incorporated – in this case, incorporation of the organic molecules typically seeks the preparation of new optical devices. However, fluorescent dyes can also be used as probes to characterize the surrounding chemical environment. Thus, fluorescence spectroscopy data can be analyzed in terms of polarity[17–19] whereas time-resolved and anisotropy measurements can be analyzed in terms of viscosity (data regarding the local frictions of the entrapped dyes can even be obtained).[20]

In this work, we focus on the study of the allocation of the organic additives within the ormosil cage through the analysis of oxazine 1 fluorescence spectroscopy, time-resolved and anisotropy measurements. Apparent microviscosities were calculated from the fluorescence anisotropy measurements in an attempt to provide information regarding the characteristic properties of the microenvironment surrounding the dye at the pore cage of the silica matrix. Knowledge regarding the dye mobility at the porous cage of different sol–gel matrices enabled us to determine the applicability of the resulting materials; for instance, photochromic[16] or photorefractive materials[21,22] need molecular rearrangements in order to work properly, whereas a fully constrained dye might be useful as a solid fluorescent standard.[20,23] FT-IR and ^{29}Si NMR spectroscopy, together with scanning electron microscopy (SEM), have also been used for the determination of the distribution of the organic additives within the ormosil cage. However, it will be seen that limited information can be obtained from these classical spectroscopic tools in this sort of study.

Experimental

Materials

Tetramethylorthosilicate (TMOS), methyl methacrylate (MMA), hydroxyethyl methacrylate (HEMA), lauryl methacrylate (LMA), polyoxyethylene(5) nonylphenyl ether (POE-5) and polyoxyethylene(40) nonylphenyl ether (POE-40) were from Aldrich. Oxazine 1 was from Kodak. Spectrophotometric grade methanol was from Merck. Water was distilled and deionized (DDW).

Sample preparation

TMOS-based gel-glass was prepared from 15.2 mmol of TMOS, 60.8 mmol ($r_{w/m}=4$) of H_2O, 65 mmol of methanol and 1.5×10^{-5} mmol of oxazine 1. The mixture was allowed to stir for 30 min in order to achieve a homogeneous solution. The polymerization was carried out at room temperature in a glass bottle covered with aluminum foil. The aluminum foil was perforated *ca.* 5 days later (after gelation) to allow the slow evaporation of the solvents, resulting in the formation of a monolithic xerogel. The sample was kept in the dark.

Ormosil gel-glasses were prepared in the same way: by mixing 15.2 mmol of TMOS, 60.8 mmol ($r_{w/m}=4$) of H_2O, 65 mmol of methanol and 1.5×10^{-5} mmol of oxazine 1. To this mixture, polyoxyethylenic-type surfactants such as POE-5 or POE-40, but also acrylic monomers as MMA, HEMA or LMA, were added in variable weight percentages (10–30%, weight organic/weight $SiO_2\times100$). The mixture was allowed to stir for 30 min in order to obtain a homogeneous solution. The polymerization was, once again, carried out at room temperature in glass bottles covered with aluminum foil, the aluminum foil being perforated *ca.* 5 days later (after gelation) to allow the slow evaporation of the solvents until the formation of monolithic xerogels. These samples were also kept in the dark. The materials thus prepared are not expected to be mesoporous or of highly ordered and uniform porosity since the experimental conditions described above differ from those characteristics for the preparation of such mesoporous materials.

Therefore, typical characterization of mesoporous materials (*e.g.* XRD or adsorption isotherms) has been omitted in this work.

Instrumentation

UV–VIS spectroscopy. A Varian UV–VIS spectrophotometer, model 2300, was used to measure absorption spectra in reflectance mode.

Infrared spectroscopy (FT-IR). Infrared spectra were obtained using a Nicolet FT-IR spectrophotometer model 20SXC. Samples were in the form of mixed KBr–gel-glass discs.

Nuclear magnetic resonance spectroscopy (^{29}Si NMR). High resolution ^{29}Si CP/MAS NMR spectra were recorded using a Bruker MSL 400 spectrometer equipped with a Fourier Transform unit. The external magnetic field was adjusted at 9.4 T. Spectra were recorded at 79.94 MHz, 5.5 s, 90° pulse width (CP), 1 ms contact time, and 5 s recycle time. The spinning frequency unit at the magic angle (54° 44′ MAS) was 4 kHz. The chemical shifts were expressed in ppm with reference to the TMS (tetramethylsilane) signal. There are four possible resonance peaks for silica gels in the ^{29}Si NMR spectra: these resonance peaks are denoted Q_1, Q_2, Q_3 and Q_4, and they correspond, respectively, to the structures $(RO)_3$–Si–$(OSi)_1$, $(RO)_2$–Si–$(OSi)_2$, $(RO)_1$–Si–$(OSi)_3$ and Si–$(OSi)_4$. Typical chemical shifts for these structures are between −82 and −86 ppm, −91 and −95 ppm, −99 and −103 ppm and at −110 ppm, respectively. Where R is a hydrocarbon chain, chemical shifts values become more negative, while the opposite behavior (less negative values) is observed where R = H.[24–27]

Scanning electron microscopy (SEM). The microstructural, morphological characteristics of the silica gels were observed by scanning electron microscopy (SEM) using a Zeiss DSM-950 instrument.

Specific surface area measurements (BET method). Specific surface area (S_A, BET method) measurements were obtained using an Omnisorp-100 (Coulter). Samples were treated under vacuum at 40–60 °C overnight, prior to the nitrogen gas adsorption.

Spectroscopy, lifetime and anisotropy measurements. Multifrequency modulation, phase analysis and fluorimetric measurements were performed at 25 °C on a 48000s SLM-Aminco spectrofluorometer (T-Optics), as described elsewhere.[28,29] Multifrequency phase and modulation fluorescence spectroscopy[30] were used for lifetime measurements (Fig. 1). The rotational reorientation kinetics were obtained from the frequency-domain anisotropy decays, as described elsewhere.[31–33] The accuracy of the lifetimes, as well as of the anisotropy measurements, was determined according to the lower χ^2_R value (the reduced error) found in each individual measurement.[34,35]

Results and discussion

1. FT-IR, ^{29}Si NMR spectroscopy and SEM of oxazine 1-doped silica gel-glasses and ormosils

Fig. 2 shows the FT-IR spectra of a TMOS-based gel-glass and a POE-5-based ormosil. Bands ascribed to silica are observed in both spectra:[36–38] Si–O–Si asymmetric bond stretching at 1088 and 794 cm^{-1}, Si–O–Si bending at 456 cm^{-1}, SiO–H stretching at 3440, Si–OH or Si–O strectching at 950 and 560 cm^{-1}, and H_2O molecules adsorbed on to the silica surface at 3440 cm^{-1} and 1620–1660 cm^{-1}. FT-IR spectra of the POE-5-based

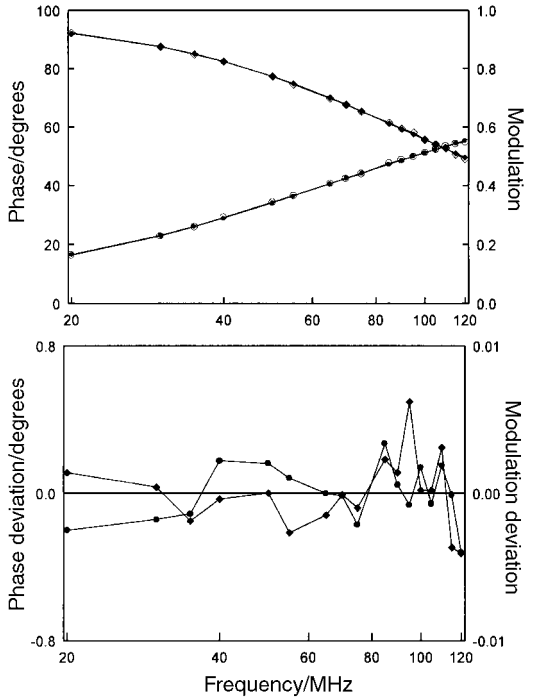

Fig. 1 Lifetime measurement of oxazine 1 (6.50×10^{-5} M)-doped gel-glass by phase and modulation methods. Top: frequency (in MHz)-dependent measured phase (●) and modulation (◆) data. Calculated phase (○) and modulation (◇) data are based on the best one-component fit. Bottom: frequency (in MHz) dependence deviations of the experimental phase (●) and modulation (◆) data from the calculated phase and modulation.

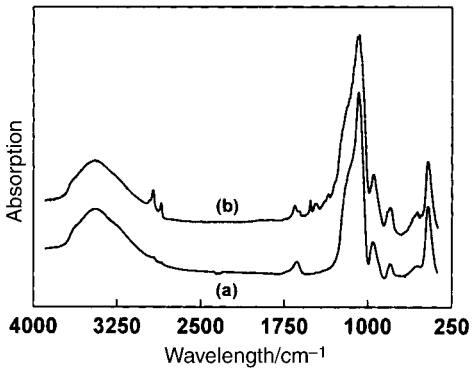

Fig. 2 FT-IR spectra of (a) TMOS-based gel-glass and (b) POE-5-based ormosil.

ormosil also show bands in range 2936–2826 cm^{-1}, which are characteristic of C–H vibrations. The C–O–C asymmetric bond stretching in linear chains vibrates at 1150–1085 cm^{-1}, and it is not observed since it is likely overlapped by the very intense band resulting from the Si–O–Si asymmetric bond stretching. Moreover, the appearance of a small band at 810 cm^{-1}, as a shoulder of the more intense band at 792 cm^{-1}, indicates the presence of Si–OR groups,[39–41] though in a smaller proportion than Si–OH groups as denoted by the high intensity of the band at *ca.* 3400 cm^{-1}. The major proportion of Si–OH groups is also supported by the chemical shift found for the Q_3 species of the POE-5-based ormosils in the ^{29}Si NMR spectrum (Fig. 3). This chemical shift is quite similar to that found for the TMOS gel-glass (−101.6 ppm *versus* –101.8 ppm, respectively), in which Si–OR groups are totally hydrolyzed as can be seen in the FT-IR spectrum (Fig. 2). The presence of Q_3 species in both the TMOS-based gel-glass as well as in the POE-5-based ormosil is indicative of non-fully condensed matrices, *i.e.* porous matrices. The appearance of the Q_3

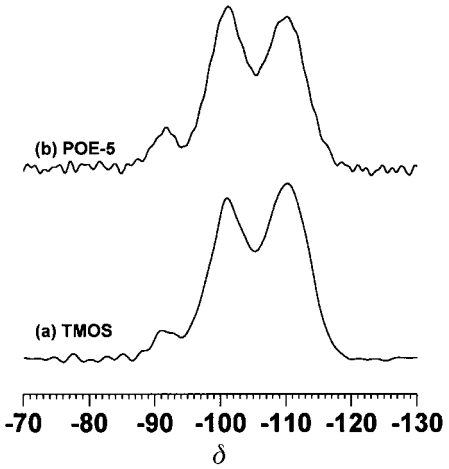

Fig. 3 ^{29}Si NMR spectra of (a) TMOS-based gel-glass and (b) POE-5-based ormosil.

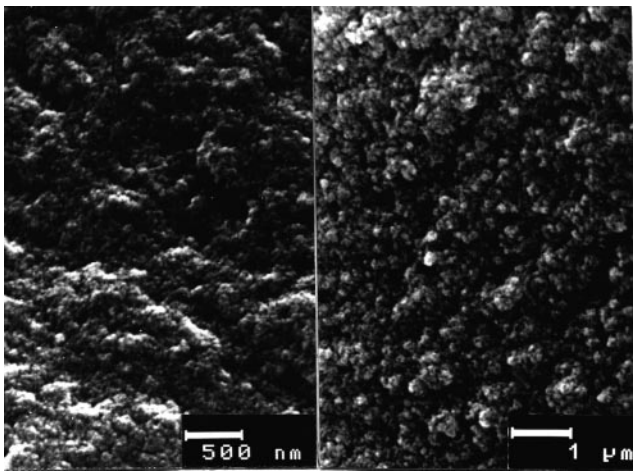

Fig. 4 SEM images of TMOS-based gel-glass (left) and POE-5-based ormosil (right).

species is a characteristic of SiO_2 matrices prepared by sol–gel methods,[41–43] since the preparation is done at room temperature (even Q_2 species in lower amounts can be observed at -92.7 ppm). A detailed discussion regarding the presence of Si–O–R groups in sol–gel silica matrices can be found in a previous work of our group.[41]

The microstructure of the gel-glass and ormosils has been studied through microscopy. The SEM images shown in Fig. 4 do not reveal large differences between the different samples, *i.e.* a typical particulate matrix resulting from a sol–gel process is observed for both samples.

Based on the above, it can be said that the results coming from spectroscopy and microscopy do not provide complete information for the determination of the distribution that the organic components adopt within the porosity of the silica matrix. Therefore, this type of study may need of a different approach. In these cases, fluorescence may be a powerful tool for the characterization of the samples. The description and analysis of the fluorescent study carried out on a number of ormosils is detailed below.

2. Fluorescence spectroscopy and time-resolved fluorescence of oxazine 1-doped silica gel-glasses

The fluorescence behavior observed for oxazine 1 doped into gel-glasses is characteristic for molecules adsorbed on to a porous silica surface, *i.e.* red shifts in the absorption and emission spectra (Fig. 5) and higher lifetime values as compared with those obtained in solution.[44,45] The suitability

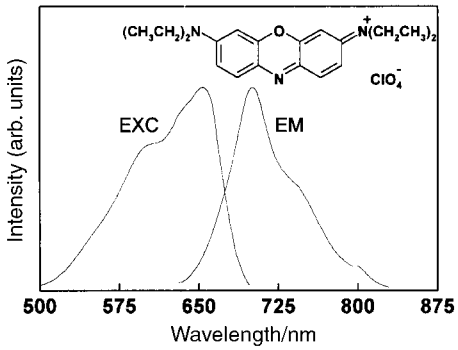

Fig. 5 Absorption and emission spectra of oxazine 1 (6.50×10^{-5} M)-doped TMOS-based gel-glass.

Table 1 Specific surface area measurements (S_A/m^2 g^{-1}) for TMOS-based gel-glass and ormosils

TMOS	HEMA	LMA	POE 5	POE40
485	347	278	324	585

Table 2 Lifetime values (τ), emission maximum wavelengths (λ_{emm}) and absorption maximum wavelengths (λ_{abm}) of oxazine 1-doped, TMOS-based gel-glasses for different oxazine 1 concentrations

[Oxazine 1]/M	τ/ns	χ^2_R	λ_{emm}/nm	λ_{abm}/nm
3.75×10^{-5}	2.35 ± 0.18	0.7	699	653
6.50×10^{-5}	2.52 ± 0.19	1.1	700	653
2.60×10^{-4}	2.60 ± 0.15	0.5	700	653
6.00×10^{-4}	2.40 ± 0.21	1.3	704	653

of oxazine 1 as a fluorescent probe for this system needs to be carefully checked. It has been reported that for dyes adsorbed on to a porous surface, changes of S_A may result in the undesired formation of dimers or aggregates.[28,29] Since changes of S_A are quite usual when surfactants or monomers are incorporated (Table 1),[12] the use of a dye that is not sensitive to concentration effects is required.

Thus, the fluorescent properties of gel-glasses doped with oxazine 1 at concentrations ranging from 3.75×10^{-5} to 6.0×10^{-4} M were firstly studied in this work, with non-significant changes of the photophysical behavior of oxazine 1 being observed (Table 2). This behavior is in good concordance with data previously reported for oxazine 1 in solution.[46] In addition, oxazine 1 has shown good chemical stability when incorporated in solid matrices.[44,45] Based on the above, oxazine 1 was chosen by the authors as a suitable fluorescent probe for the achievement of this work.

3. Steady-state and time-resolved fluorescence of oxazine 1 in non-ionic surfactant-based ormosils

Spectroscopic data are shown in Table 3. Special attention was paid to the Stokes shifts (the difference between the emission and absorption maxima; $\Delta\lambda=\lambda_{emm}-\lambda_{abm}$, in nm) since they showed more interesting information than the analysis of the absorption and emission spectra separately.[47] The origin of the polarity dependence of the Stokes shifts is the dipole relaxation of the excited state of the probe. After absorption of an incident photon an excited state is obtained with a different dipole moment than that from the ground state. The spatial distribution of the dipoles around the excited state is initially out of equilibrium, which is reached after a relaxation time. If the relaxation time is less than the fluorescence lifetime, then a final relaxed state is obtained before the fluorescence emission. The difference in energy between the initial and the relaxed states is dependent upon the polarity of the medium.

Table 3 Lifetime values (τ), emission maximum wavelength (λ_{emm}), absorption maximum wavelengths (λ_{abm}) and Stokes shifts ($\Delta\lambda$) for oxazine 1-doped ormosils ([oxazine 1] = 6.50×10^{-5} M)

Sample	τ/ns	χ^2_R	λ_{emm}/nm	λ_{abm}/nm	$\Delta\lambda$/nm
TMOS	2.52±0.19	1.1	700	653	47
POE-5 10%	2.85±0.22	1.7	697	654	43
POE-40 10%	3.05±0.18	1.0	698	653	45
POE-5 20%	3.60±0.20	1.5	696	—	—
POE-5 30%	3.85±0.21	1.7	697	—	—
MMA 10%	2.33±0.17	0.8	694	655	39
HEMA 10%	2.35±0.21	1.4	704	657	47
LMA 10%	2.96±0.20	1.3	700	659	41
MMA 20%	2.52±0.19	1.1	696	—	—
HEMA 20%	2.72±0.25	2.3	704	—	—
HEMA 30%	2.95±0.20	1.4	704	—	—

Thus, experimental data given in Table 3 show shorter Stokes shift values when oxazine 1 is incorporated into POE-5- and POE-40-based ormosils than when it is incorporated into TMOS-based gel-glasses. According to that mentioned above, such behavior indicates an increase in polarity of the surrounding dye environment. Also, compared to TMOS-based gel-glasses, an increase of the oxazine 1 lifetime values was observed for the non-ionic surfactant-based ormosils (Table 3). Moreover, the lifetime for oxazine 1 doped in the POE-40-based ormosil was larger than that for oxazine 1 doped in the POE-5 matrix. Since the non-polar tail of both non-ionic surfactants is quite similar, then the observed difference in the lifetime value must be related to the length of the polyoxyethylenic chain, *i.e.* the longer the polyoxyethylenic chain, the larger the lifetime value. The lifetime modifications must, therefore, be analyzed in terms of viscosity rather than of polarity.

The relationship between the number of polyoxyethylenic units and lifetime values was corroborated by the measurement of the oxazine 1 lifetime in ormosils prepared with an increased POE-5 concentration (20–30%, Table 3). Lifetime measurements therefore indicate that the interaction of the non-ionic surfactants with the porous silica surface must be through the polar head, while the non-polar tail is oriented in the opposite direction to the surface (Fig. 6). Furthermore, the polyoxyethylenic chains must be adsorbed in a tangled fashion on the surface rather than linearly, which will determine a higher coverage of the adsorption surface since the size of the polar head is greater (Fig. 6). These results are in good accord with reported data from adsorption isotherms, EPR, Raman or NMR spectroscopy, regarding the adsorption behavior of amphiphilic molecules on polar surfaces (not necessarily prepared by sol–gel).[48–53]

The increase in viscosity mentioned above should somehow impede any molecular rearrangement of the fluorescent probe at the ormosil cage. Fluorescence anisotropy measurements of oxazine 1-doped gel-glasses and ormosils will better illustrate how oxazine 1 is constrained within the pores of these gel-glasses and ormosils (see below, Section 4).

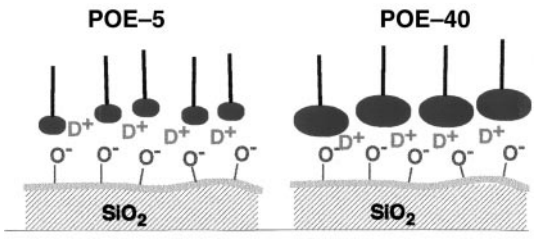

Fig. 6 Schematic representation of the distribution of POE-5 (a) and POE-40 (b) on the ormosil cage as indicated by the photophysical properties of oxazine 1.

4. Steady-state and time-resolved fluorescence of oxazine 1 in acrylic monomer-based ormosils

Ormosils based on the incorporation of acrylic monomers (MMA, HEMA and LMA) as non-ionic additives were also studied. The Stokes shifts measured for oxazine 1 in MMA-based ormosils were shorter than those in TMOS-based gel-glasses (Table 3). It is known that when acrylic monomers are incorporated to a silica gel, interactions between the carbonyl groups of the monomers and the silanol groups at the silica surface take place through hydrogen bonding.[4] The presence of the carbonyl group close to the porous surface results in an increase in the polar character surrounding the dye, as revealed in the measured Stokes shifts. On the other hand, the measured Stokes shifts of oxazine 1 doped in HEMA-based ormosils (Table 3) indicate a decrease in polar character of the dye environment as compared with that observed in MMA-based ormosils. The Stokes shift values of oxazine 1 doped in LMA-based ormosils were between those observed for MMA and HEMA, though closer to MMA than to HEMA. The largest Stokes shift that is observed for HEMA-based ormosils must be a consequence of the, already reported,[54] partial re-esterification of the polar Si–OH groups with the hydroxy groups of HEMA , which do not take place for either MMA or LMA. Therefore, oxazine 1 is mainly probing polarity changes at the polar silica surface rather than those arising from the long, non-polar chain of LMA which is out of the polar surface.

The lifetime values of oxazine 1 measured in the MMA, as well as in the HEMA-based ormosils, were similar to those previously observed for oxazine 1 in TMOS-based gel-glasses. On the other hand, larger lifetime values were observed for oxazine 1 in LMA-based ormosils (Table 3). Moreover, the lifetime values measured for oxazine 1 with increased MMA/HEMA concentrations (MMA 20%, HEMA 20–30%, Table 3) showed high lifetime values, similar to those observed for LMA (10%)-based ormosils. The lack of non-polar chains linked to the MMA/HEMA acrylic monomer points out that oxazine 1 lifetimes are more likely reflecting viscosity changes arising from the presence of large molecules (LMA) or higher monomer concentrations (MMA/HEMA).

As mentioned above, such an increase in the viscosity at the ormosil cage should somehow impede the mobility of the oxazine 1. Fluorescence anisotropy of these samples was also performed (see below) to better determine this assessment.

5. Fluorescence anisotropy of oxazine 1-doped ormosils

Calculated values of the steady-state fluorescence anisotropy,[20,55] $\langle r \rangle$, of oxazine 1 are reported at the xerogel state both for the oxazine 1-doped, TMOS-based gel-glasses as well as for the oxazine 1-doped ormosils studied above (Table 4). These $\langle r \rangle$ values are higher than those previously reported[56] for oxazine 1 in titania-based gel-glasses, where oxazine 1 was modeled as a single rotator in a low viscous environment, *i.e.* water from the hydrolysis reaction that remains at the porous cage.[56] The differences mentioned above are related to the different isoelectric points of titania and silica (*ca.* 5–6 and *ca.* 2–3, respectively[57,58]). Unlike silica, the porous surface of titania-based gel-glasses can be considered as a positively-charged surface, and electrostatic forces should locate the cationic dye (oxazine 1) not too close to the surface. Similar behavior has also been reported for aluminosilicate gels,[59] which are also positively-charged.

In our case, the measurement of a high $\langle r \rangle$ value reflects the partially hindered or slowed down dynamics of the probe as a consequence of its favored adsorption on the negative, porous surface of the silica gel-glasses and ormosils. The similar $\langle r \rangle$ values found both for oxazine 1 in TMOS-based gel-glasses as well as in ormosils indicate a similar situation of the dye within

Table 4 Lifetime values (τ) and steady-state fluorescence anisotropy ($\langle r \rangle$) obtained for oxazine 1-doped, TMOS-based gel-glasses and ormosils ([oxazine 1] = 6.50×10^{-5} M). Initial anisotropy (r_0), rotational correlation time (Φ), fractional contribution (α), residual anisotropy (r_∞) and chi-squared (χ^2_R) have also been included by the application of different models to the fluorescence anisotropy data

	TMOS	MMA 10%	HEMA 10%	POE-5 10%
τ/ns	2.52 ± 0.19	2.33 ± 0.17	2.35 ± 0.21	2.85 ± 0.22
$\langle r \rangle$	0.311 ± 0.003	0.311 ± 0.003	0.321 ± 0.003	0.311 ± 0.003
Single exponential decay model				
r_0	0.4	0.385	0.372	0.385
Φ/ns	13.7	17.5	15.2	23.8
χ^2_R	10.4	12.3	11.5	10.9
Two exponential decay model				
r_0	0.4	0.399	0.4	0.378
Φ_1/ns	0.54	0.07	0.36	0.33
α_1 (%)	25	15	19	16
Φ_2/ns	19.9	14.6	19.6	23.4
χ^2_R	1.2	1.3	1.2	1.1
Hindered rotator model				
r_0	0.377	0.357	0.385	0.350
r_∞	0.226	0.152	0.195	0.170
Φ/ns	2.53	7.54	5.13	7.08
χ^2_R	1.1	1.2	1.0	0.9

these matrices.[56] Furthermore, the measured $\langle r \rangle$ values were below the fundamental anisotropy value expected for vitrified systems,[60] indicating that the dye is not totally constrained by the pore cage but still keeps a certain degree of mobility. These results are in good agreement with those reported for rhodamine 6G (R6G; cationic dye)[31] and also for PRODAN (neutral dye)[32] doped into gel-glasses, *i.e.* higher $\langle r \rangle$ values than in solution but lower than in vitrified systems.

Nevertheless, steady-state anisotropy measurements provide only an insight into the average environment about the fluorescent probe; it is possible to recover the underlying rotational motions and to estimate local microviscosities from time-resolved anisotropy. For excited species in a single type isotropic environment, the decay of anisotropy, $r(t)$, is given by a linear combination of exponentially decaying functions[55,61]

$$r(t) = r_0 \sum \beta_i \exp(-t/\phi_i) \quad (1)$$

where $\Sigma\beta_i = 1$, and where β_i is the fractional contribution of total depolarization, ϕ_i is the rotational correlation time attributed to a motion i, and r_0 is the fundamental anisotropy which depends on the angle between the absorption and emission transition moments. The maximum value of r_0 is reached when the emission and absorption transition dipoles are parallel, and it has been theoretically calculated as 0.4.[60] This information has been used to see whether or not the similar values found for $\langle r \rangle$ correspond to true, dynamically similar environments.

The experimental data fitted to eqn. (1) for $i = 1$, 2 and 3 are presented in Table 4. Fitting of the data to a single exponential decay, which describes the anisotropy function of an *isotropic* probe, gave chi-squared values far from unity for all of the samples. Better fits were found for the two exponential decay model, which describes the anisotropy function of an *anisotropic* rotator. In this case, the two exponential decay model has already been considered in rhodamine 6G doped in TMOS gel-glasses,[31] the faster exponential decay being related to those molecules solvated with remaining solvents and the slower exponential decay to those molecules adsorbed on the porous surface. The two exponential decay model was considered inappropriate in this case. Otherwise, two distinguishable lifetimes (*ca.* 0.8 ns and *ca.* 2.5 ns[44,46]) reflecting the presence of oxazine 1 in such different environments (solvated in remaining solvents and adsorbed on the porous surface, respectively) would have been measured in this work. As a matter of fact, taking into account the electrostatic attraction between oxazine 1 and the silica surface, it seems more plausible to consider that the oxazine 1 is adsorbed mostly on the porous silica surface, rather than being solvated in remaining solvents. Further fitting with three exponential decays ($i = 3$) did not improve the quality of the analysis. At this situation, the experimental data could be better modeled as a hindered rotator [eqn. (2)]

$$r(t) = [(r_0 - r_\infty) \exp(-t/\Phi)] + r_\infty \quad (2)$$

where r_∞ is the residual anisotropy, and is related to the cone angle of the wobbling and contains information about the order parameter. In this model, the apparent relaxation time Φ is given by

$$\Phi = \frac{\sigma}{D_W} \quad (3)$$

where D_W is the wobbling diffusion constant and σ is a constant that depends solely upon the value of r_0/r_∞, *i.e.* upon the angle of wobbling.[62]

In Table 4 we present the anisotropy parameters obtained for oxazine 1 in doped, TMOS-based gel-glasses and in ormosils using a hindered rotator model. The goodness of the fitting to a spatially hindered rotator model is corroborated by the low value of chi-squared (Table 4). In all cases, the $\langle r \rangle$ values calculated from the recovered parameters for the anisotropy decay using the hindered model were in good agreement with the measured $\langle r \rangle$ values within the experimental error.[56] In addition, the average value of the recovered fundamental anisotropy was 0.379, which is very close to the predicted fundamental anisotropy for a probe with a high symmetry.[60]

It is known that in systems with strong interactions between the probe and the surface of aggregates (micelles) or the cavity cage in polymers, non-zero anisotropy (r_∞) values are observed.[56] This value implicitly contains information about the order of the environment, reflecting the degree of orientational constraint due to the surrounding media, *i.e.* the higher the r_∞ value, the stronger the orientational constraint of the fluorescent probe. Thus, the high r_∞ values observed in TMOS-based gel-glasses indicate probe adsorption on the matrix surface.

Regarding the acrylic monomer-based ormosils, a high r_∞ value was found for HEMA-, as compared with MMA-based, ormosils. This high r_∞ value was attributed to the re-esterification of the Si–OH groups at the surface with the hydroxy group belonging to HEMA,[54] which would confine the probe in a more restricted orientational domain. On the other hand, the low r_∞ value observed for MMA, as well as for POE-5, indicated a higher degree of disorder as a consequence of the larger amplitude ability with which the probe can be reoriented.

As mentioned above, in the hindered model the apparent rotational correlation time is a function of the diffusion constant, but it also contains information about the order parameter sensed by the probe. The experimental D_W value can be obtained from eqn. (2) and (3) and it is possible to estimate the local microviscosity, η, sensed by the probe using a modified form of the Stokes–Einstein–Debye equation,[55,61]

$$D_W = \frac{kT}{6\eta f V_{eff}} \quad (4)$$

where k is the Boltzmann constant, T is the temperature, V_{eff} is the effective volume which includes the Perrin shape factor which takes into account the asymmetry of the rotating object, and f is a dimensionless factor that depends on the friction mechanism. For stick boundary conditions $f = 1$.

Table 5 σ Values, wobbling diffusion constants (D_W) and local microviscosities (η) obtained for oxazine 1-doped, TMOS-based gel-glasses and ormosils

Sample	σ	D_W/ns^{-1}	η/cP
TMOS	0.081	0.032	37
MMA 10%	0.111	0.015	82
HEMA 10%	0.097	0.019	64
POE-5 10%	0.101	0.014	85

The wobbling diffusion constant values (Table 5) were obtained for TMOS-based gel-glasses and some ormosils from eqn. (3) through the polynomial approximation of the σ values as a function of the experimentally determined r_∞/r_0 values [eqn. (5)]:[62,63]

$$\sigma = 0.1674 - 0.10661(r_\infty/r_0) - 0.062(r_\infty/r_0)^2 \quad (5)$$

The effective volume has been calculated in a previous work[56] as a revolution ellipsoid ($V_{eff} = 564$ Å^3) assuming the molecule shape is a prolate ellipsoid. Table 5 shows the local 'apparent' microviscosities calculated from eqn. (4).

The recovered 'apparent' microviscosity data showed higher values for all ormosils studied than for TMOS-based gel-glasses, in good agreement with previous results found for rhodamine 6G-doped TMOS/PEG [poly(ethylene glycol)] materials.[64] Furthermore, such an increase in viscosity is in good accordance with the increase of the lifetime values observed above (Sections 2 and 3). The differences between the microviscosity values calculated in this work from oxazine 1 and those previously reported for rhodamine 6G[31] must likely be related to the model employed in the data analysis.

The fluorescence anisotropy data measured for oxazine 1 in the TMOS-based gel-glass, as well as in the ormosils, show that the fluorescent probe retains a certain degree of mobility within the porous cage. It has been demonstrated that elucidation of the distribution of the organic additives within the porosity of the ormosils can be attempted through calculation of the apparent microviscosity of the environment surrounding the dye, though large differences were not observed in the present study.

Conclusion

Steady-state and time-resolved fluorescence of oxazine 1 have been used to determine the distribution of dopant molecules at the porous surface of the ormosil cage. Fluorescence has been shown as a very useful tool for the characterisation of ormosil matrices, rather than classical spectroscopic tools such as FT-IR or ^{29}Si NMR. In addition, the non-destructive character of fluorescence makes the use of this technique a very convenient approach to apply in the study of many organic–inorganic hybrid materials.

The fluorescence anisotropy measurements have been fitted according the hindered rotator model. The goodness of this fitting corroborates that oxazine 1 strongly interacts with the silanol groups of the porous surface. According the recovered 'apparent' microviscosity data, oxazine 1 seems to be in a more restricted environment at the ormosil than it is at the gel-glass cage. Nevertheless, anisotropy data have also shown that such an interaction does not fully inhibit the mobility of oxazine 1 within the porosity of any of the studied matrices.

Based on the results presented above, these ormosils seem to be more suitable hosts as fluorescent standards, where dye mobility must be more restricted than with photochromic or photorefractive materials, where molecular rearrangements are required. Nevertheless, further work is currently in progress for the achievement of matrices capable of better confining fluorescent dyes.

Acknowledgements

The authors are grateful to CICYT for the research grant ESP98-1332-C04-04. The authors are also grateful to Professor C. R. Mateo for her valuable discussions and to C. Alonso for technical support. Maria L. Ferrer is grateful to CAM for a postdoctoral fellowship.

References

1 E. J. A. Pope and J. D. Mackenzie, *J. Non-Cryst. Solids*, 1986, **87**, 185.
2 G. Philipp and H. Schmidt, *J. Non-Cryst. Solids*, 1984, **63**, 283.
3 H. Schmidt, *J. Non-Cryst. Solids*, 1985, **73**, 681.
4 X. Li and T. A. King, *SPIE, Sol–Gel Optics III*, 1994, **2288**, 216.
5 A. Julbe, C. Balzer, J. M. Barthez, C. Guizard, A. Labort and L. Cot, *J. Sol–Gel Sci. Technol.*, 1995, **4**, 89.
6 C. Sanchez and F. Ribot, *New J. Chem.*, 1994, **10**, 987.
7 C. J. Brinker and G. W. Scherer, *Sol–Gel Science*, Academic Press, San Diego, 1990
8 S. Sakka, *J. Non-Cryst. Solids*, 1985, **73**, 651.
9 C. J. Brinker, *J. Non-Cryst. Solids*, 1988, **100**, 651.
10 D. R. Ulrich, *J. Non-Cryst. Solids*, 1988, **100**, 174.
11 L. L. Hench and J. K. West, *Chem. Rev.*, 1990, **90**, 33.
12 C. T. Kresge, M. E. Leonowicz, W. J. Roth, J. C. Vartuli and J. S. Beck, *Nature*, 1992, **359**, 710.
13 N. K. Raman, M. T. Anderson and J. C. Brinker, *Chem. Mater.*, 1996, **8**, 1682.
14 D. Avnir, D. Levy and R. Reisfeld, *J. Phys. Chem.*, 1984, **88**, 5956.
15 B. Leveau, N. Herlet, J. Livage and C. Sanchez, *Chem. Phys. Lett.*, 1993, **206**, 15.
16 D. Levy and D. Avnir, *J. Phys. Chem.*, 1988, **92**, 4734.
17 E. W. Castner Jr., M. Maroncelli and G. R. Fleming, *J. Chem. Phys.*, 1987, **86**, 1090.
18 M. Maroncelli and G. R. Fleming, *J. Chem. Phys.*, 1987, **86**, 6221.
19 D. Ben-Amotz and J. M. Drake, *J. Chem. Phys.*, 1988, **89**, 1019.
20 J. R. Lackowicz, *Topics in Fluorescence Spectroscopy: Principles*, Plenum Press, New York, 1991, vol. 2.
21 B. Darracq, M. Canva, F. Chaput, J. P. Boilot, D. Riehl, Y. Levy and A. Brun, *Appl. Phys. Lett.*, 1997, **70**, 292.
22 W. E. Moerner and S. M. Silence, *Chem. Rev.*, 1994, **94**, 127.
23 J. R. Lackowicz, *Topics in Fluorescence Spectroscopy: Probe Design and Chemical Sensing*, Plenum Press, New York, 1994, vol. 4.
24 F. Babonneau, L. Bois and J. Livage, in *Better Ceramics Through Chemistry V*, ed. M. J. Hampden-Smith, W. G. Klemperer and C. J. Brinker, *Mater. Res. Soc. Symp. Proc.*, 1992, **271**, 237
25 F. Brunet and B. Cabane, *J. Non-Cryst. Solids*, 1993, **163**, 211.
26 H. Kaji, K. Nakanishi and N. Soga, *J. Non-Cryst. Solids*, 1995, **181**, 16.
27 B. M. De Witte, D. Commers and J. B. Uytterhoeven, *J. Non-Cryst. Solids*, 1996, **202**, 35.
28 F. del Monte and D. Levy, *J. Phys. Chem. B*, 1998, **102**, 8036.
29 F. del Monte and D. Levy, *J. Phys. Chem. B*, 1999, **103**, 8080.
30 J. R. Lackowicz, G. Laczko, H. Cherk, E. Gratton and M. Limkeman, *Biophys. J.*, 1984, **46**, 462.
31 U. Narang, R. Wang, P. N. Prasad and F. V. Bright, *J. Phys. Chem.*, 1994, **98**, 17.
32 U. Narang, J. D. Jordan, F. V. Bright and P. N. Prasad, *J. Phys. Chem.*, 1994, **98**, 8101.
33 H. Soyez, M. Huang, B. S. Dunn and J. I. Zink, *SPIE, Sol–Gel Optics IV*, 1997, **3136**, 118.
34 P. R. Bevington, *Data Reduction and Error Analysis for the Physical Sciences*, McGraw-Hill Inc., New York, 1969, p. 336
35 E. Gratton and M. Linkeman, *Biophys. J.*, 1983, **44**, 315.
36 R. M. Almeida, T. A. Guiton and G. C. Pantano, *J. Non-Cryst. Solids*, 1990, **121**, 193.
37 F. G. Galeener, *Phys. Rev. B*, 1979, **19**, 4292.
38 M. Ocaña, V. Fornes and C. J. Serna, *J. Non-Cryst. Solids*, 1989, **107**, 187.
39 Y. Abe, T. Namiki, K. Tuchida, Y. Nagao and T. Misono, *J. Non-Cryst. Solids*, 1992, **147–148**, 47.
40 D. Niznansky and J. L. Rehspringer, *J. Non-Cryst. Solids*, 1995, **180**, 191.
41 F. del Monte and D. Levy, *Opt. Mater.*, 1999, **13**, 17.
42 M. J. Peeters, W. J. J. Wakelkamp and A. P. M. Kentgens, *J. Non-Cryst. Solids*, 1995, **186**, 77.
43 U. Damrau and H. C. Marsman, *J. Non-Cryst. Solids*, 1994, **168**, 42.

44 F. del Monte and D. Levy, *SPIE, Sol–Gel Optics III*, 1994, **2288**, 276.
45 F. del Monte and D. Levy, *Chem. Mater.*, 1995, **7**, 292.
46 M. F. Quinn, M. S. Al-Ajeel and F. Al-Bahrani, *J. Lumin.*, 1985, **33**, 53.
47 D. L. Bernik and R. M. Negri, *J. Colloid Interface. Sci.*, 1998, **203**, 97.
48 P. Nilsson, H. Wennerström and B. Lindman, *J. Phys. Chem.*, 1983, **87**, 1377.
49 F. Tiberg and M. Landgren, *Langmuir*, 1993, **9**, 927.
50 R. Strey, R. Schomäcker, D. Roux, F. Nallet and U. J. Olsson, *J. Chem. Soc., Faraday Trans.*, 1990, **86**, 2253.
51 M. R. Böhmer, L. Koopal, K. R. Janssen, E. M. Lee, R. K. Thomas and A. R. Rennie, *Langmuir*, 1992, **8**, 2228.
52 P. Somasundaran and J. Y. Kunjappu, *Colloids Surf.*, 1989, **37**, 245.
53 P. Quist and E. Soderlind, *J. Colloid Interface. Sci.*, 1995, **172**, 510.
54 F. del Monte and D. Levy, *J. Sol–Gel Sci. Technol.*, 1997, **8**, 585.
55 J. R. Lackowicz, *Principles of Fluorescence Spectroscopy*, Plenum Press, New York, 1983, ch. 5
56 M. C. Marchi, A. A. Bilmes and R. M. Negri, *Langmuir*, 1997, **13**, 3665.
57 J. C. Pouxviel, B. Dunn and J. I. Zink, *J. Phys. Chem.*, 1989, **93**, 2134.
58 R. Rodriguez, M. A. Blesa and A. E. Regazzoni, *J. Colloid Interface Sci.*, 1996, **177**, 122.
59 B. S. Dunn and J. I. Zink, *J. Mater. Chem.*, 1991, **1**, 903.
60 R. E. Dale, in *Time Resolved Fluorescence Spectroscopy in Biochemistry and Biology*, ed. R. B. Cundall and R. E. Dale, *NATO ASI Ser., Ser. A: Life Sciences*, Plenum Press, New York, 1983, vol. 69, pp. 605–606
61 R. F. Steiner, in *Topics in Fluorescence Spectroscopy: Principles*, ed. J. R. Lackowicz, Plenum Press, New York, 1991, vol. 2, ch. 1
62 K. Kinoshita, S. Kawato and A. Ikegami, *Biophys. J.*, 1977, **20**, 289.
63 C. R. Mateo, A. A. Souto, F. Amat-Guerri and A. U. Acuña, *Biophys. J.*, 1996, **71**, 2177.
64 G. A. Baker, J. D. Jordan and F. V. Bright, *J. Sol–Gel Sci. Technol.*, 1998, **11**, 43.